Melting and Shedding of Graupel and Hail. Part I: Model Physics

ROY M. RASMUSSEN* AND ANDREW J. HEYMSFIELD

*National Center for Atmospheric Research,** Boulder, CO 80307*

(Manuscript received 20 March 1986, in final form 7 April 1987)

ABSTRACT

A detailed model of the melting, shedding, and wet growth of spherical graupel and hail is presented. This model is based upon recent experimental studies by Rasmussen et al. and Lesins et al. The model is presented in the form of five easy-to-use tables. Important quantities considered were the heat transfer, terminal velocity behavior, and shedding of liquid water.

1. Introduction

Previous studies on the evolution of hail in convective storms have concentrated on processes by which hail can grow to large sizes within a storm's lifetime (Browning and Ludlam, 1962; List, 1963; Browning, 1963; Bailey and Macklin, 1968; Heymsfield, 1982; and Heymsfield 1983a). In general, recent modeling efforts using three-dimensional (3-D) Doppler-derived wind fields in conjunction with detailed hail growth models (Paluch, 1978; Heymsfield 1983b; Foote, 1984) have shown that our current knowledge of hail growth seems to be sufficient to reproduce many of the main features of hail growth. In contrast, relatively little attention has been given to the physics of hail melting, wet growth, and the shedding of liquid water. Melting is critical to determining final hail size and terminal velocity at the ground, while shedding can be an important source of new raindrops (Wisner et al., 1972) which may subsequently serve as new hailstone embryos (Rasmussen and Heymsfield, 1987b).

Wet growth is an important process which can significantly affect the growth rate and terminal velocity of hail (Lesins et al., 1980). Current parameterizations of melting hailstones in the kinematic models described above and in dynamical cloud models (Wisner et al., 1972; Orville and Kopp, 1977; and Cotton et al., 1982) are based on the work by Mason (1956) and Macklin (1963). The major limitations of Mason and Macklin's studies were that only graupel (<0.5 cm diameter) and large hailstones (>3 cm diameter) were considered, and these were not falling at terminal velocity. The recent experimental studies on melting by Rasmussen and Pruppacher (1981) and Rasmussen et al. (1984a,b; hereafter referred to as RLPa,b) have significantly extended these results by allowing a wide range of particle sizes (0.3–2.5 cm diameter) to melt at terminal velocity.

Wet growth parameterizations typically do not allow for spongy growth, and assume that either all unfrozen water is shed (Dennis and Musil, 1973; Orville and Kopp, 1977) or all unfrozen water retained (English, 1973). Recent laboratory studies by Lesins et al. (1980) and Joe et al. (1976) have greatly improved on our knowledge of wet growth. In this study we will present a detailed model of melting, shedding, and wet growth based upon the experimental results of RLPa,b and Lesions et al. (1980). Sensitivity studies using this model will be presented in Part II (Rasmussen and Heymsfield, 1987a). In Part III, we apply this model to a particular case study (Rasmussen and Heymsfield, 1987b).

2. Model physics

The detailed microphysical model presented in the following sections (based upon the model by Heymsfield, 1982) allows individual particles, whether hail, graupel, snowflakes, or single crystals, to evolve by condensational growth, 2) dry riming growth, 3) wet growth, 4) evaporation, and 5) melting. In this paper, we will emphasize aspects of the model concerning the evolution of spherical hail[1] and graupel by melting, shedding and wet growth. Shedding of water drops is allowed to occur in both wet growth and melting. The specific atmospheric environmental conditions of temperature, pressure, relative humidity, and liquid water content are specified before a model run. In most cases, these conditions are obtained from rawinsonde soundings or aircraft data. For a summarized form of the model parameterization, see Tables 1 to 4 and Fig. 1.

* Current affiliation: Bureau of Reclamation, Denver Federal Center, Box 25007, Denver, CO 80225.

** The National Center for Atmospheric Research is funded by the National Science Foundation.

[1] Matson and Huggins (1980), for instance, found that 84% of the hailstones they observed in free fall were spheroidal.

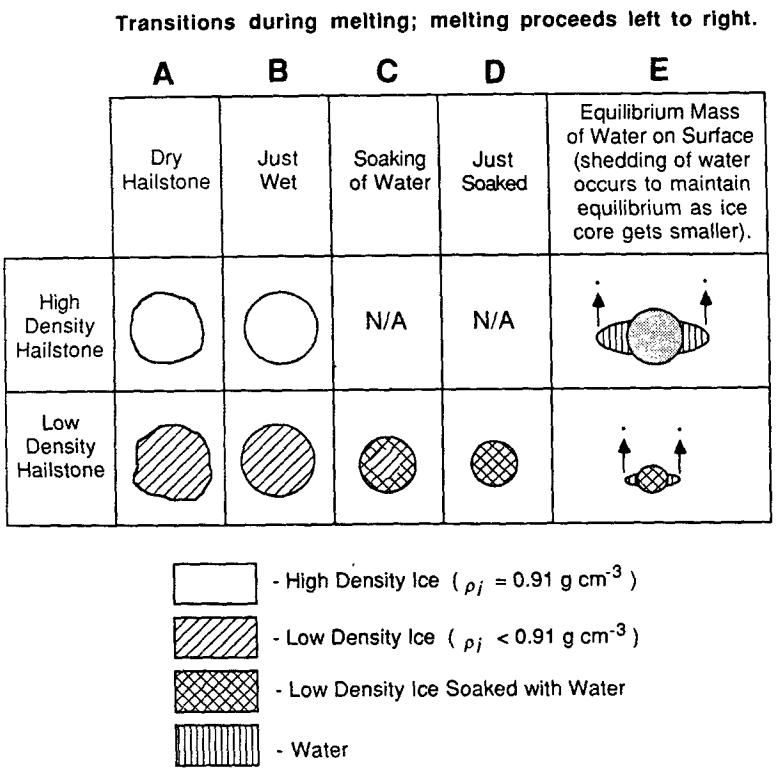

FIG. 1. Schematic diagram showing the stages of melting experienced by high- and low-density ice particles. The left-most panel shows a dry particle; panels progressively to the right show the stages encountered with increasing melting. The density of the particle refers to the initial ice density. Columns D and E represent hailstones with a density between ice and water.

a. Melting equations

1) HEAT TRANSFER

The transfer of heat to melting spherical hailstones depends on the stage of melting. Equations describing the heat transfer in each of the four stages discussed by RLPab are shown in Table 1, with symbols defined in appendix A. Equations (1) and (2) represent the melting stage in which the ice core is completely embedded within a spherical shell of meltwater. In this Reynolds number regime the meltwater is circulating, causing the heat transfer to be enhanced. The meltwater in this stage is not shed. Equation (3) represents the melting stage in which the meltwater does not circulate due to the oblate shape of the melting particle. Due to the lack of circulation, heat transfer is reduced. The ice core is still embedded in the meltwater during this stage, and meltwater is not shed. Note that the equation given by RLPb to cover the Reynolds number range 3.0×10^3–6.0×10^3 has been replaced here with an equation originally derived by Mason (1956). This equation is much simpler to use than the equation suggested by RLPb, and gives sufficient accuracy within the indicated Reynolds number range. Equation (4) represents the melting stage during which most of the meltwater is shed. For Reynolds number greater than 2×10^4 the heat transfer coefficient, χ, as given by Bailey and Macklin (1968) for rough spheres has been used [Eq. (5)]. This coefficient increases rapidly with Reynolds number, and is essential for the growth of large hailstones (Rasmussen and Heymsfield, 1987b).

The basic quantity predicted from these equations is the change in radius of the ice core, a_i, with time as a function of the environmental conditions:

$$4\pi\rho_i a_i^2 L_m \frac{da_i}{dt} = \frac{dq}{dt}. \quad (1)$$

The density used, ρ_i, in this equation and in the model, is the bulk ice density of the particle.

2) TERMINAL VELOCITY

The following discussion relates to the problem of calculating terminal velocity aloft.

(i) Equilibrium terminal velocity. As shown by RLPb, the melting process often leads to a significant decrease in a particle's terminal velocity. They observed a torus of water to build up near the equator of their solid ice sphere during melting, increasing its cross-sectional area, and consequently decreasing its terminal velocity. Once the torus became thick enough, shedding of water drops occurred. This resulted in a further de-

TABLE 1. Heat transfer equations for melting hailstones and graupel. Relations for $\bar{f}_h, \bar{f}_v$, L_e, L_m, D_v, k_a and k_w are given in Table A1. The expression $(dm/dt)_{cd}$ is the mass growth rate through collection of cloud droplets. Equation (3) is solved by an iterative solution to the heat balance equation.

Applicable Reynolds number range	Heat transfer equation	No.
$N_{Re} < 250$	$dq/dt = (-4\pi a_d k_a (T_\infty - T_0)\bar{f}_h - 4\pi a_d L_e D_v(\rho_{v,\infty} - \rho_{v,0})\bar{f}_v)2.0 - c_{p,w}(T_\infty - T_0)(dm/dt)_{cd}$	(1)
$2.5 \times 10^2 \leq N_{Re} \leq 3 \times 10^3$	$dq/dt = -4\pi a_d k_a (T_\infty - T_0)\bar{f}_h - 4\pi a_d L_e D_v(\rho_{v,\infty} - \rho_{v,0})\bar{f}_v - c_{p,w}(T_\infty - T_0)(dm/dt)_{cd}$	(2)
$3.0 \times 10^3 < N_{Re} < 6 \times 10^3$	$dq/dt = \dfrac{4\pi a_d a_i k_w [T_0 - T_a(a_i)]}{(a_d - a_i)} = -4\pi a_d k_a [T_\infty - T_d(a_i)]\bar{f}_h - 4\pi a_d L_e D_v(\rho_{v,\infty} - \rho_{v,a})\bar{f}_v - c_{p,w}(T_\infty - T_a)(dm/dt)_{cd}$	(3)
$6 \times 10^3 \leq N_{Re} \leq 2 \times 10^4$	$dq/dt = -\chi 2\pi a_i N_{Re}^{1/2}[N_{Pr}^{1/3} k_d (T_\infty - T_0) + N_{Sc}^{1/3} L_e D_v(\rho_{v,\infty} - \rho_{v,0})] - c_{p,w}(T_\infty - T_0)(dm/dt)_{cd}$ where $\chi = 0.76$	(4)
$N_{Re} > 2 \times 10^4$	Same as Eq. (4) but $\chi = 0.57 + 9.0 \times 10^{-6} N_{Re}$	(5)

crease in terminal velocity due to the loss of mass. For particles with Reynolds number greater than 1.0×10^4, shedding tends to occur as a result of the air flow shearing off liquid from the torus. Below this Reynolds number, shedding occurs as a result of the instability of the water torus (similar to the spontaneous breakup of large raindrops). In the following we refer to the terminal velocity behavior after the onset of shedding as "equilibrium terminal velocity."

Observations by Matson and Huggins (1980) of melting hailstones in free fall also suggest that terminal velocities during melting are lower. The drag coefficients they determined for hailstones collected in northeast Colorado were 50% higher than those for the same sized rough sphere, but consistent with horizontally oriented, oblate hailstones. Photographs of these hailstones in free fall indicated an average axis ratio that agreed well with those determined by Knight (1984) for hailstones larger than 1.3 cm diameter (collected at the ground in northeast Colorado), while for hailstones smaller than 1.3 cm diameter, Matson and Huggins's axis ratios became progressively more oblate than those given by Knight. This suggests that the formation of a water torus due to melting was occurring for these sizes. Photographs of the ice cores (presented in Matson and Huggins) also revealed the characteristic "Bayer aspirin" pill shape as found by RLPb for their melting ice spheres. Further observations along these lines, however, need to be done in order to confirm this behavior.

In RLPb's study, they examined the change in terminal velocity for a 1.84-cm diameter solid ice sphere melting at sea level. A reexamination of their data showed that the Reynolds number of a melting particle *once it starts to shed,* can be expressed as a linear function of the mass of ice remaining for Reynolds numbers between 5×10^3 and 2.5×10^4:

$$N_{Re_{iM}} = 4800.0 + 4831.5 \cdot M_i. \quad (2)$$

This equation was determined using linear regression, and has a correlation coefficient of 0.99 with the laboratory data. This equation, however, strictly applies only to sea level conditions. In order to extend this equation to other conditions and heights in the atmosphere, we use an approach suggested by McDonald (1960) and confirmed by Beard (1976) for raindrops. This method is valid for particles whose shape is invariant with changing atmospheric conditions.

This approach begins with the balance between a particle's drag and weight:

$$D = C_D \frac{1}{2} \rho_a U_\infty^2 A_c = mg, \quad (3)$$

where A_c is the cross-sectional area of the particle, and D is the total drag. Consider now the same particle at two different levels in the atmosphere. Since mg remains nearly the same, the total drag at these two locations will be the same, and we can therefore write the following equation:

$$C_{D_1} \frac{1}{2} \rho_{a_1} U_{\infty_1}^2 A_{c_1} = C_{D_2} \frac{1}{2} \rho_{a_2} U_{\infty_2}^2 A_{c_2}, \quad (4)$$

where subscript 1, 2 refers to level 1, 2. If the particle's shape is preserved with altitude, then $A_{c_1} = A_{c_2}$ (cross-sectional areas are equal), and we can solve for the terminal velocity at level 2:

$$U_{\infty_2}^2 = \frac{C_{D_1}}{C_{D_2}} \frac{\rho_{a_1}}{\rho_{a_2}} U_{\infty_1}^2. \quad (5)$$

If the ratio (C_{D_1}/C_{D_2}) can be determined at the two levels, then (5) can be solved. Since the drag curves for spheroids of different axis ratio are similar in their functional form (Beard, 1976), we may estimate this ratio from the corresponding ratio for smooth spheres at these two levels. The critical question, then, is whether the invariance of shape (i.e., cross-sectional

area and axis ratio) with different atmospheric conditions can be shown.

The shape of water drops falling in air is mainly determined by a balance of the internal hydrostatic pressure gradient and the surface tension, independent of the aerodynamic pressures and atmospheric conditions (Beard, 1976). This means that a melting particle's shape is also likely to be invariant with altitude for $N_{Re} \leq 5 \times 10^3$ because it rapidly melts into the raindrop shape for these Reynolds numbers. For higher Reynolds numbers, shape is determined by the build-up of a water torus by the shear stress at the particle's surface. This shear stress is proportional to the Bernoulli pressure, $\frac{1}{2}\rho_a U_\infty^2$, in (3). Consider a large spherical ice core uniformly coated with water released from rest in still air of density ρ_a. The Bernoulli pressure, and therefore the shear stress, will increase with increasing U_∞. Water will start to be dragged upwards toward the particle's equator. Water from the rear, downstream region of the particle will have a tendency to move upstream under the influence of gravity towards the region of flow separation near the particle's equator. This process will result in an increase of the cross-sectional area, as well as the drag coefficient, since the drag coefficient of spheroids increases with increasing oblateness (List et al., 1973). Since the drag coefficient for a given spheroid varies very slowly with N_{Re} (Clift et al., 1978, p. 145) in the range $3 \times 10^3 \leq N_{Re} \leq 3 \times 10^5$, an increase of C_D with oblateness will occur in this Reynolds number range. Thus, C_D and A_c for the above-considered particle will increase with $\frac{1}{2}\rho_a U_\infty^2$, (for the above Reynolds number range), until the total drag D, balances the weight, mg. Because of this, C_D is only related to the axis ratio (and therefore A_c) of the oblate spheroid. Since C_D in this case is only a weak function of atmospheric conditions, there will be only one value of $\frac{1}{2}\rho_a U_\infty^2$, independent of altitude, which will balance the particle's weight at terminal velocity (C_D and A_c depend upon each other).

This leads to the general result that a given particle will have unique values of C_D and A_c for given $\frac{1}{2}\rho_a U_\infty^2$, and that the balance condition when $D = mg$ will have unique values of $C_D A_c$, and $\frac{1}{2}\rho_a U_\infty^2$. Since $D = C_D \frac{1}{2}\rho_a U_\infty^2 A_c$ is invariant with altitude [Eq. (4)], C_D, A_c, and $\frac{1}{2}\rho_a U_\infty^2$ will also be invariant with altitude. This in turn, means that the shape of a melting particle will tend to be invariant with altitude, allowing use of (5) to calculate the terminal velocity of melting particles at any atmospheric condition. The specific algorithm used for this calculation is summarized in Tables 2 and 3 under the "equilibrium mass of water on surface" category (see also Fig. 1, E).

(ii) Terminal velocity during initial phase transition. The terminal velocity estimates developed in the preceding section only give a method to calculate the *equilibrium* terminal velocity of a melting particle (see Fig. 1, E). In the following we consider the transition of the terminal velocity from a dry particle to a particle in equilibrium.

Let us first consider the transition from a dry to a just-wet hailstone, without a significant change in shape (Fig. 1, B). One might expect intuitively that wet hailstones have lower drag coefficients than dry ones. Macklin and Ludlam (1961) showed experimentally, however, that the drag coefficient of a wet-ice model with $4 \times 10^4 \leq N_{Re} \leq 1.6 \times 10^5$ did not differ signifi-

TABLE 2. Terminal velocity of wet high-density hailstones.

Surface state		Terminal velocity relationship
1) Just wet*	$N_{Re} > 4000$	Drag coefficient for dry hailstone (appendix B)
	$N_{Re} \leq 4000$	Smooth sphere drag coefficient (appendix B)
2) Transition from "just wet" to "equilibrium mass of water on surface"		Linear interpolation between "just wet" terminal velocity and terminal velocity calculated assuming the equilibrium amount of water on surface. Interpolation based upon fraction of equilibrium water on surface.
3) Equilibrium mass of water on surface		
$N_{Re} < 5000$		Terminal velocity of raindrops following Beard (1976)
$5 \times 10^3 \leq N_{Re} \leq 2.5 \times 10^4$		$U_{\infty_2}^2 = C_{D_1}\rho_{a_1} U_{\infty_1}^2 / (C_{D_2}\rho_{a_2})$ (1)
		where subscript 1 refers to sea level, and subscript 2 to any arbitrary height and $U_{\infty_1} = \frac{(4800.0 + 4831.5 M_i)0.15}{2a_d}$
		$\frac{C_{D_1}}{C_{D_2}}$ = ratio of the drag coefficients for spheres of the same mass and size at sea level and the arbitrary height (Beard, 1976)
$N_{Re} > 2.5 \times 10^4$		Assume a drag coefficient of 0.6 (nearly all water shed).

* Just wet refers to the surface state of the hailstone immediately after passing from the dry stage to the wet stage (surface temperature is equal to 0°C).

TABLE 3. Terminal velocity of wet low-density* hailstones (graupel).

Surface state	Terminal velocity relation
1) Just wet	
$N_{Re} > 4000$	Drag coefficient for dry graupel (appendix B)
$N_{Re} \leq 4000$	Smooth sphere drag coefficient (appendix B)
2) Soaking of water	Drag coefficient as in "Just Wet" stage
3) Just soaked	If $\rho_i > 0.8$, drag coefficient for dry graupel (Appendix B) If $\rho_i \leq 0.8$, drag coefficient for smooth sphere (Appendix B)
4) Transition from "just soaked" to "equilibrium mass of water on surface"	Linear interpolation between "just soaked" terminal velocity and the terminal velocity calculated assuming the equilibrium mass of water on surface. Interpolation based on the fraction of water on surface compared to equilibrium amount on surface
5) Equilibrium mass of water on surface	
$N_{Re} < 5000$	Terminal velocity of raindrops following Beard (1976)
$5 \times 10^3 \leq N_{Re} \leq 2.5 \times 10^4$	$U^2_{\infty_2} = C_{D_1}\rho_{a_1}U^2_{\infty_1}/(C_{D_2}\rho_{a_2})$ (1) where subscript 1 refers to sea level and subscript 2 to any arbitrary height and $U_{\infty_1} = \dfrac{(4800.0 + 4831.5M_s)0.15}{2a_d}$ $\dfrac{C_{D_1}}{C_{D_2}}$ = ratio of the drag coefficients for spheres of the same mass at sea level and the arbitrary height M_s = sum of M_i and soaked water
$N_{Re} > 2.5 \times 10^4$	Assume a drag coefficient of 0.6 (nearly all water shed)

* The density referred to is the initial ice density.

cantly from the drag coefficient when the ice model was dry. The fact that surface roughness has very little effect on the drag of a large hailstone can be deduced from the experimental work by Achenbach (1972) on spheres. He found that the skin-friction component of the drag for smooth spheres between $3 \times 10^3 \leq N_{Re} \leq 3 \times 10^5$ was only 1% to 10% of the total drag. The overall drag of the particle was mainly determined by the particle's shape (form drag). Thus, even a 100% increase in the skin-friction drag (roughness) will have only a minimal effect on the drag of these large spheres. For lower Reynolds numbers, however, Selberg and Nicholls (1968) have shown that roughness can significantly increase the drag coefficient. This follows because the drag coefficient of low Reynolds number spheres have a strong dependence on the skin-friction component. For instance, for $N_{Re} = 300$, the skin-friction component of the drag is 47% of the total drag (LeClair et al., 1972).

This behavior led us to base our terminal velocity transition from a dry to a wet surface on the Reynolds number. For Reynolds numbers greater than 4000, we assume no change in the drag coefficient from a dry hailstone. For Reynolds numbers less than 4000, the drag coefficient of the wet hailstone or graupel is assumed to be that of a smooth sphere (Fig. 1, column B). A summary of this procedure for graupel and hail is presented in Tables 2 and 3 under the category "just wet."

Since we often have low-density particles of high Reynolds number melting (e.g., Knight and Heymsfield, 1983), an additional transition is necessary. As stated earlier, for high Reynolds numbers, the shape of the particle mainly determines the drag coefficient, assuming that the particle assumes the same orientation with respect to the airflow. After a low-density particle is fully soaked with water, the shape may be significantly affected because the soaked meltwater can be aerodynamically molded such that it does not conform to the exterior of the ice core. We therefore allow transition to a smooth sphere for $N_{Re} \geq 4000$ if the density of ice is less than 0.8 g cm^{-3} (see Fig. 1, B). This behavior is summarized in Table 3 under the category: just soaked.

Finally, we still have to consider the transition between a just-wet hailstone or graupel and a hailstone or graupel with the equilibrium amount of water on its surface (Fig. 1, C). This is done by linear interpolation between the just-wet terminal velocity, and the terminal velocity calculated for the particle assuming that it has the equilibrium amount of water on its surface (Table 2 under: transition from just wet to equilibrium).

When low-density graupel are melting, we first allow the particle to completely soak with water (Kidder and Carte, 1964; Prodi, 1970) (see Fig. 1, C and D), after which the particle transforms to the equilibrium-sized particle (Fig. 1, E). During this transition, we assume

the terminal velocity of a smooth sphere (Table 3 under: transition from just soaked to equilibrium).

3) AXIS RATIO

Calculations of axis ratio used in Part II of this study are based on the melting results of RLPb. The parameterization uses the mass of water accumulated on the surface and the mass of the ice core plus any soaked water as the basic predictor. The axis ratio is then determined from the figures presented in RLPb. The present calculation assumes that the particles are not colliding with other particles, and that turbulence levels are low.

b. Shedding equations

1) MELTING

The experiments of RLPb have shown that melting ice spheres shed part of their meltwater (in the form of water drops) if their initial diameter is greater than 9 mm (at sea level). For the present study, we have taken their results on shedding and formulated an equation relating the mass of the ice core to the mass of water on its surface:

$$M_{w_{crit}} = 0.268 + 0.1389 M_i \qquad (6)$$

where $M_{w_{crit}}$ is the mass of water on the ice core's surface just before shedding occurs. This equation is valid for melting ice spheres shedding at sea level. A plot of this equation is shown as the upper line in Fig. 2. The lower line is a plot derived from the theoretical work of Chong and Chen (1974). The experiments by RLPb observed much more water being retained by the ice core than predicted by Chong and Chen. These two studies represent the two extreme behaviors expected, nearly all water shed versus large amounts of liquid water retained under stable flow conditions.

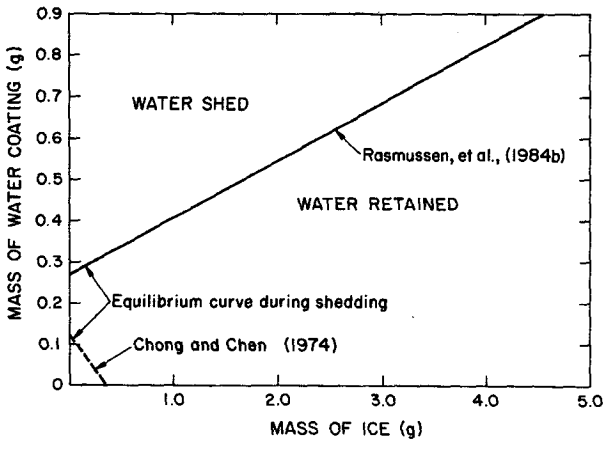

FIG. 2. Experimental (Rasmussen et al., 1984b) and theoretical (Chong and Chen, 1974) predictions of the equilibrium mass of water coating for given mass of spherical, 0.91 g cm^{-3} density, ice core during melting or wet growth. By equilibrium we are referring to the maximum amount of water mass which can coat the ice core before shedding. Above the respective lines water is shed, while below the respective lines water is retained.

Equation (6) implies there is a maximum amount of water which can be retained on the surface of a given ice core mass before shedding (the "equilibrium" amount). If the amount of water exceeds this maximum amount, we allow shedding of the excess water to occur. This permits a very simple description of the shedding process.

If low-density graupel are melting, we first allow the meltwater to completely soak (all air spaces occupied) the graupel (Kidder and Carte, 1964), (Fig. 1, D), and then allow accumulation of water on the surface (Fig. 1, E). The ice core mass used in Eq. (6) is calculated as the sum of the ice plus any soaked water.

Equation (6), however, only applies to the experimental conditions of RLPb. What happens when we bring the same particle into other atmospheric conditions? This problem can be addressed by referring back to the previous section on terminal velocity. In that section we determined that for $N_{Re} > 4000$, a given distribution of ice core mass and accumulated water will maintain the same Bernoulli pressure and cross-sectional area with altitude. Since shedding for these high Reynolds numbers depends mainly on the surface shear stress and shape, the shedding behavior of the melting hailstones should be independent of altitude. For $N_{Re} \leqslant 4000$, shedding does not depend on the shear stress, but on Rayleigh–Taylor instability (RLPb). Since this mechanism depends only on the mass of water present, this shedding mechanism is also independent of altitude. This allows us to use (6) in calculating the maximum stable amount of surface water for a given ice core mass for any atmospheric condition and Reynolds number. Since the meltwater is always close to 0°C, the temperature variation of surface tension is not important for these calculations. It must also be remembered that these results apply only to non-tumbling hail. It has not been determined conclusively if melting hail does or does not tumble. RLPb observed that a water torus tended to stabilize its particles during the initial stages of melting. Free-fall hydrodynamic motions were restricted however, by the size of the tunnel. Blanchard (1955) allowed a 2-cm diameter ice sphere to melt in free fall in a wind tunnel and found that the water torus which formed around the particle's equator tended to stabilize it. Russian wind tunnel experiments on melting hail in free fall also suggest that tumbling motions do not occur (Gvelesiani and Kartsivadze, 1968). They observed melting hail to move in a helical fall pattern of one meter diameter, with the water torus oriented horizontally at all times (Tlisov, private communication). This also makes physical sense because the water torus is fluid, and able to adjust to any new orientation of the hailstone. This parameterization, however, does not consider the effects of horizontal wind shear, turbulence, or collisions between

particles. Further experiments are needed to determine if these effects are important.

2) WET GROWTH

In many ways, wet growth is analogous to melting. Wet growth occurs on a hailstone when all the accreted water is not immediately frozen, but accumulates on or within the hailstone. In the following we distinguish between two separate parameterizations of wet growth, "high-density wet growth" and "spongy wet growth."

(i) High-density wet growth. In this case, we assume all frozen water has a density of 0.91 g cm^{-3}. All unfrozen water is assumed to accumulate on the particle's surface. Terminal velocity and shedding are calculated in the same manner as during melting.

(ii) Spongy wet growth. Spongy growth of hail occurs when "that portion of the collected water which immediately freezes produces a skeletal framework . . . of dendritic ice crystals in which the unfrozen portion of the collected water is retained as in a sponge whose surface temperature is at 0° Celsius" (Pruppacher and Klett, 1980). During this type of wet growth, water is assumed to freeze with a low density (0.48–0.75 g cm^{-3}), within which the unfrozen portion of the collected water is retained. If the volume of unfrozen water is greater than the soakable volume, water is allowed to accumulate on the hailstone's surface based on Eq. (6). The mass of the ice core used to calculate the equilibrium mass of water on the surface (Eq. 6) is considered to be the mass of ice plus any soaked water.

Whether or not hailstones tumble or gyrate during *wet* growth has not been determined. Mossop and Kidder (1962) found that for artificial hailstones suspended rigidly but kept at terminal velocity with a drag balance, spongy growth became aerodynamically molded into a belt around the equator, similar to that found by Blanchard (1955) and RLPb for melting ice spheres. This type of aerodynamic molding of spongy growth was also found by Kidder and Carte (1964) as well as by List (1959). If the spongy ice layer is semifluid, it may be able to inhibit tumbling or gyration in the same manner as suggested for melting hail. If there is more unfrozen water than can be soaked into the low-density ice matrix, a water torus may develop which will also tend to stabilize tumbling.

On the other hand, if the spongy ice layer is not fluid enough, tumbling or gyrating motions may develop, as suggested by List et al. (1973), Thwaites et al. (1977), and Knight and Knight (1970). List et al. suggest that gyrating motions become more likely as a particle becomes more oblate, which indeed occurs with aerodynamic molding of spongy growth.

The above discussion shows that the free-fall behavior of hailstones undergoing spongy growth is not very well understood. The fact that shedding of liquid water occurs during spongy growth, however, has been well documented by many studies (Kidder and Carte, 1964; Carras and Macklin, 1973; Joe et al., 1976; Lesins et al., 1980; Joe and List, 1984). These shedding results, however, are from rigidly mounted cylinders and spheres, and from spheres with prescribed gyration. Carras and Macklin (1973) do include results for one hailstone falling at terminal velocity in their tunnel, but these data are not sufficient to permit generalization to arbitrary atmospheric conditions. In light of the inadequate knowledge on both the fall behavior and shedding of hailstones undergoing spongy growth, we are forced to make a best guess as to their actual behavior in formulating a parameterization of spongy growth. In formulating this parameterization, we will attempt to determine the *minimum* amount of mass shed during spongy growth, and use the best available data.

One of the more complete studies on shedding during spongy growth was conducted by Lesins et al. (1980). They conducted icing experiments on rotating cylinders for a wide range of liquid water contents (2–40 g m^{-3}), air temperatures (−2 to −20°C), and rotation rates (2–30 Hz), but all at a constant air velocity of 18 m s^{-1} and initial cylinder diameter of 1.9 cm. This airspeed and cylinder diameter, however, are typical of conditions in clouds under which hailstones are shedding. We will therefore base much of our parameterization on this study.

One of the important parameters that needs to be determined is the density of the ice matrix. This is given by Lesins et al. (1980) as a function of the fraction of the total accreted deposit frozen, called I, the ice fraction. They found that for cylinder rotation rates of 0.5 Hz, the ice fraction depends only on LWC, and not on air temperature in the temperature range −4° to −16°C. They also found that water was shed in this case from a 3 mm bulge near the equator, similar to the torus observed by RLPb during melting.

For rotation rates of 5–7 Hz, the ice fraction reached a minimum. Shedding also reached a minimum, reflected in the bulge in the water skin becoming smaller. This rotation rate allowed more of the water to become trapped in the ice matrix, and less to accumulate in the bulge. Nearly all shedding was observed to originate from this water bulge, similar to that observed during the melting of ice spheres by RLPb. For higher rotation rates, shedding was observed to increase as the centrifugal force was now strong enough to overcome surface tension forces. These higher rotation rates also left unrealistic spikes which are not observed for natural hailstones. Realistic features were observed for rotation rates less than about 10 Hz.

As stated earlier, we would like to parameterize the minimum amount of water shed by a hailstone in spongy growth. We therefore reduced the ice fraction frozen for a rotation rate of 0.5 Hz by 0.2 in order to better agree with the minimum ice fraction at 5–7 Hz, where shedding was also a minimum, and the growth

TABLE 4. Wet growth parameterization.

1. High-density wet growth
   All frozen water has a density of 0.91 g cm^{-3}.
2. Spongy wet growth
   Spongy growth is assumed to have a density of:

$$\rho_{\text{spongy}} = (1.0 - 0.08I)I \quad (1)$$

where I is the ice fraction given by:

$$I = I_0 + [(1 - I_0)/(1 + K_I(W_f - W_I))] - 0.2 \quad W_f \geq 2\,\text{g m}^{-3} \quad (2)$$

$$I = 1 \quad W_f < 2\,\text{g m}^{-3} \quad (3)$$

where

$I_0 = 0.25$
$K_I = 0.1798\,\text{g m}^{-3}$
$W_I = 2.0\,\text{g m}^{-3}$

and W_f is the liquid water content in g m^{-3}.

The ice fraction represents the fraction of a water mass frozen.

pattern fairly realistic. Table 4, Eq. (2) shows the ice fraction equation, and Eq. (1), Table 4, the density of the spongy ice matrix. The water not frozen is soaked into the ice matrix, and any excess water allowed to accumulate in a bulge near the particle's equator. We then use the shedding parameterization developed for melting spheres to determine when the mass of the bulge exceeds the equilibrium mass. Any water in excess of the equilibrium size is shed.

3. Conclusions

A comprehensive melting and wet-growth parameterization has been presented which describes the

1) heat transfer
2) changes in terminal velocity, and
3) shedding of water drops

experienced by hailstones as they fall through regions of the atmosphere which causes their surface temperature to be greater than or equal to 0°C (air temperatures greater than 0°C or high liquid water contents). The parameterization is presented in the form of five easy-to-use tables.

Acknowledgments. The authors would like to thank Frances Huth for all her time and effort spent on typing, editing, and revising these documents. We would also like to thank Dr. David Johnson for his helpful comments and suggestions on the original manuscripts. Comments by Dr. R. List, R. Farley, and an anonymous reviewer greatly improved the paper.

APPENDIX A

List of Symbols

a_d	overall radius of particle
a_i	radius of ice core
A_c	cross-sectional area perpendicular to the flow
C_D	drag coefficient
$c_{p,w}$	heat capacity of water
D	total drag
D_v	diffusivity of water vapor in air
$\bar{f}_h$	mean ventilation coefficient for heat
$\bar{f}_v$	mean ventilation coefficient for water vapor
g	gravitational acceleration
I	ice fraction
I_0	constant equal to 0.25
k_a	thermal conductivity of air
k_w	thermal conductivity of water
k_I	constant equal to 0.1798 g m^{-3}
K_a	thermal diffusivity of air
L_e	latent heat of evaporation
L_m	latent heat of melting
M_i	mass of ice core
m	total mass of particle
$M_{w_{\text{crit}}}$	critical mass of water on ice core just before the onset of shedding
N_{Re}	Reynolds number ($=2a_dU_\infty/\nu$)
$N_{\text{Re}_{iM}}$	Reynolds number of a melting particle after the onset of shedding
N_{Pr}	Prandtl number ($=\nu/K_a$)
N_{Sc}	Schmidt number ($=\nu/D_v$)
q	heat content

TABLE A1.

$$L_e = 597.3\left(\frac{273.15}{T}\right)^{\gamma}, \quad \gamma = 0.167 + 3.67 \times 10^{-4}T$$

with T in °K, L_e in cal g^{-1}.

$$L_m = 79.7 + 0.485T - 2.5 \times 10^{-3}T^2$$

with T in °C, L_m in cal g^{-1}.

$$D_v = 0.211\left(\frac{T}{T_0}\right)^{1.94}\left(\frac{P_0}{P}\right)$$

with $T_0 = 273.15$°K,
$P_0 = 1013.25$ mb,
T in °K, D_v in cm^2 s^{-1}.

$$k_a = (5.69 + 0.017T) \times 10^{-5}$$

with T in °C and k_a in cal cm^{-1} s^{-1} °C^{-1}.

$$k_w = 135.8 \times 10^{-5} \exp(3.473 \times 10^{-3}T - 3.823 \times 10^{-5}T^2 + 1.087 \times 10^{-6}T^3)$$

with T in °C, k_w in cal cm^{-1} s^{-1} °C^{-1}.

$$\bar{f}_v = 0.78 + 0.308N_{\text{Sc}}{}^{1/3}N_{\text{Re}}{}^{1/2}$$

$$\bar{f}_h = 0.78 + 0.308N_{\text{Pr}}{}^{1/3}N_{\text{Re}}{}^{1/2}$$

where N_{Pr} and N_{Re} are defined in Appendix A.

Values of $\bar{f}_h$ and $\bar{f}_v$ were taken from Pruppacher and Rasmussen (1979) and L_e, L_m, D_v, k_a and k_w were obtained from Pruppacher and Klett (1980).

t time
T_a temperature (K) at the surface of the particle
T_0 constant equal to 273.16 K (triple point)
T_∞ temperature (K) in the environment far from particle's surface
U_∞ terminal velocity of the particle
W_I constant equal to 2.0 g m^{-3}
W_f liquid water content in g m^{-3}
ρ_i density of ice
ρ_a density of air
$\rho_{v,a}$ water vapor density at temperature T_a
$\rho_{v,0}$ water vapor density at temperature T_0
$\rho_{v,\infty}$ water vapor density at temperature T_∞
ν kinematic viscosity of air
η_a dynamic viscosity of air
χ heat transfer coefficient

APPENDIX B

Terminal Velocity of Dry Graupel and Hailstones

Figure 3 presents a plot of drag coefficient versus Reynolds number for 1) smooth spheres (solid line) and 2) graupel and hail. The smooth sphere plot was obtained from Clift et al. (1978), in which they used existing data to obtain a curve valid for Reynolds numbers between 1 and 10^7. The graupel and hail curve (dashed line) was based on the studies by Knight and Heymsfield (1983), Roos and Carte (1973), Roos (1972), Bailey and Macklin (1968), Young and Browning (1967), Willis et al. (1964), Macklin and Ludlam (1961), and List and Schemenauer (1971). In the present model, graupel and hail are assumed to be spherical. The terminal velocity of a particle is calculated by 1) determining the Best number $(X) = C_D N_{Re}^2 = 8mg\rho_a/(\pi\eta_a^2)$ from the mass of the particle and environmental conditions; 2) determining the particle's Reynolds number from a Best number–Reynolds number relation; and 3) solving for terminal velocity from the Reynolds number $U_\infty = \eta_a N_{Re}/(2a_d\rho_a)$.

The Best number–Reynolds number relation is determined from the drag coefficient versus Reynolds number dashed curve in Fig. 3. For graupel and hail with Reynolds number between 1 and 3 ($\times 10^5$), the relations are ($W = \log_{10} X$):

$$\log_{10} N_{Re} = 1.7095 + 1.33438W - 0.11591W^2 \qquad 73 < X < 562 \quad (1 < N_{Re} \leq 12.2), \quad \text{(B1)}$$

$$\log_{10} N_{Re} = -1.81391 + 1.34671W - 0.12427W^2 + 0.0063W^3 \qquad 562 < X \leq 1.83 \times 10^3 \quad (12.2 < N_{Re} \leq 30) \quad \text{(B2)}$$

$$N_{Re} = 0.4487X^{0.5536} \qquad 1.83 \times 10^3 < X < 3.46 \times 10^8 \qquad (30 < N_{Re} < 2.4 \times 10^4), \quad \text{(B3)}$$

$$N_{Re} = (X/0.6)^{1/2}, \qquad 3.46 \times 10^8 < X < 5.4 \times 10^{10} \qquad (2.4 \times 10^4 < N_{Re} < 3.0 \times 10^5). \quad \text{(B4)}$$

Equation (B4) is equivalent to assuming that the drag coefficient equals 0.6. The equations given for $N_{Re} \leq 30$, are based upon drag coefficients for smooth spheres. The terminal velocity behavior during critical transition and beyond are not presented here but can be found in Clift et al. (1978). The critical transition condition for hailstone growth rarely occurs (Roos, 1972).

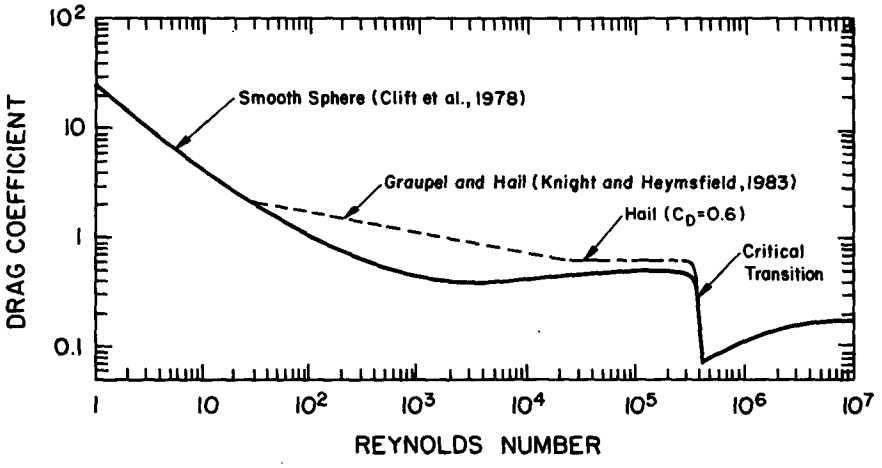

FIG. 3. Drag coefficients as a function of Reynolds number for 1) smooth spheres (solid line) and 2) graupel and hail (dashed line).

REFERENCES

Achenbach, E., 1972: Experiments on the flow past spheres at very high Reynolds numbers. *J. Fluid Mech.*, **54,** 565–575.

Bailey, I. H., and W. C. Macklin, 1968: Heat transfer from artificial hailstones. *Quart. J. Roy. Meteor. Soc.* **94,** 93–98.

Beard, K. V., 1976: Terminal velocity and shape of cloud and precipitation drops aloft. *J. Atmos. Sci.*, **33,** 851–864.

Blanchard, D. C., 1955: The supercooling, freezing, and melting of giant waterdrops at terminal velocity in air. *Proc. Conf. on Cloud and Precipitation Particles,* Pergamon Press, 233–249.

Browning, K. A., 1963: The growth of large hail within a steady updraught. *Quart. J. Roy. Meteor. Soc.*, **89,** 490–506.

——, and F. H. Ludlam, 1962: Airflow in convective storms. *Quart. J. Roy. Meteor. Soc.*, **88,** 117–135.

Carras, J. N., and W. C. Macklin, 1973: The shedding of accreted water during hailstone growth. *Quart. J. Roy. Meteor. Soc.*, **99,** 639–648.

Chong, S., and C. S. Chen, 1974: Water shells on ice pellets and hailstones. *J. Atmos. Sci.* **31,** 1384–1391.

Clift, R., J. R. Grace and M. E. Weber, 1978: *Bubbles, Drops, and Particles.* Academic Press, 380 pp.

Cotton, W. R., M. A. Stephens, T. Nehrkorn and G. J. Tripoli, 1982: The Colorado State University three-dimensional cloud/mesoscale model—1982. Part II: An ice phase parameterization. *J. Rech. Atmos.*, **16,** 295–320.

Dennis, A. S., and D. J. Musil, 1973: Calculations of hailstone growth and trajectories in a simple cloud model. *J. Atmos. Sci.*, **30,** 278–288.

English, M., 1973: *Alberta Hailstorms,* Part II. Growth of large hail in the storm. *Meteor. Monogr.*, No. 38, Amer. Meteor. Soc., 98 pp.

Foote, G. B., 1984: A study of hail growth utilizing observed storm conditions. *J. Climate Appl. Meteor.*, **23,** 84–101.

Gvelesiani, A. I., and A. I. Kartsivadze, 1968: On the melting of spherical hailstones. *Proc. Int. Conf. on Cloud Physics,* Toronto, 422–426.

Heymsfield, A. J., 1982: A comparative study of the rates of development of potential graupel and hail embryos in High Plains storms. *J. Atmos. Sci.*, **39,** 2867–2897.

——, 1983a: Case study of a hailstorm in Colorado. Part IV: Graupel and hail growth mechanisms deduced through particle trajectory calculations. *J. Atmos. Sci.*, **40,** 1482–1509.

——, 1983b: A technique for investigating graupel and hail development, *J. Climate Appl. Meteor.*, **22,** 1143–1160.

Joe, P. I., and R. List, 1984: Numerical modelling of hail to rain conversion. *Proc. Ninth Int. Cloud Physics Conf.,* Tallinn, USSR, 261–265.

——, ——, P. R. Kry, M. R. de Quervain, P. Y. K. Lui, P. W. Stagg, J. D. McTaggart-Cowan, E. P. Lozowski, M. C. Steiner, J. von Niederhausern, R. E. Stewart, E. Freire and G. Lesins, 1976: Loss of accreted water from a growing hailstone. *Proc. Int. Cloud Physics Conf.,* Boulder, 264–269.

Kidder, R. E., and A. E. Carte, 1964: Structures of artificial hailstones, *J. Rech. Atmos.*, **1,** 169–181.

Knight, C. A., and N. C. Knight, 1970: The falling behavior of hailstones. *J. Atmos. Sci.*, **27,** 672–681.

Knight, N. C., 1984: The shape factor of hailstones. *Proc. Ninth Int. Cloud Physics Conf,* Tallinn, USSR, 99–100.

——, and A. J. Heymsfield, 1983: Measurement and interpretation of hailstone density and terminal velocity. *J. Atmos. Sci.*, **40,** 1510–1516.

Leclair, B. P., A. E. Hamielec, H. R. Pruppacher and W. D. Hall, 1972: A theoretical and experimental study of the internal circulation in water drops falling at terminal velocity in air. *J. Atmos. Sci.*, **29,** 728–740.

Lesins, G. B., R. List and P. I. Joe, 1980: Ice accretions. Part I: Testing of new atmospheric icing concepts. *J. Rech. Atmos.*, **14,** 347–356.

List, R., 1959: Wachstum von Eis-Wassergemischen im Hagelversuchskanal. *Helv. Phys. Acta,* **32,** 293–296.

——, 1963: General heat and mass exchange of spherical hailstones. *J. Atmos. Sci.*, **20,** 189–197.

——, and R. S. Schemenauer, 1971: Free-fall behavior of planar snow crystals, conical graupel, and small hail. *J. Atmos. Sci.*, **28,** 110–115.

——, U. W. Rentsch, A. C. Byram and E. P. Lozowski, 1973: On the aerodynamics of spheroidal hailstone models. *J. Atmos. Sci.*, **30,** 653–661.

McDonald, J. E., 1960: An aid to computation of terminal fall velocities of spheres. *J. Meteor.*, **17,** 463–465.

Macklin, W. C., 1963: Heat transfer from hailstones. *Quart. J. Roy. Meteor. Soc.*, **89,** 360–369.

——, and F. H. Ludlam, 1961: The fallspeeds of hailstones. *Quart. J. Roy. Meteor. Soc.*, **87,** 72–81.

Mason, B. J., 1956: On the melting of hailstones. *Quart. J. Roy. Meteor. Soc.*, **82,** 209–216.

Matson, R., and A. W. Huggins, 1980: The direct measurement of the sizes, shapes and kinematics of falling hailstones. *J. Atmos. Sci.*, **37,** 1107–1125.

Mossop, S. C., and R. E. Kidder, 1962: Artificial hailstones. *Bull. Obs. Puy de Dome,* **2,** 65–80.

Orville, H. D., and F. J. Kopp, 1977: Numerical simulation of the life history of a hailstorm. *J. Atmos. Sci.*, **34,** 1596–1618.

Paluch, I. R., 1978: Size sorting of hail in a three-dimensional updraft and implications for hail suppression. *J. Appl. Meteor.*, **17,** 763–777.

Prodi, F., 1970: Measurements of local density in artificial and natural hailstones. *J. Appl. Meteor.*, **9,** 903–910.

Pruppacher, H. R., and R. Rasmussen, 1979: A wind tunnel investigation of the rate of evaporation of large water drops falling at terminal velocity in air. *J. Atmos. Sci.*, **36,** 1255–1260.

——, and J. D. Klett, 1980: *Microphysics of Clouds and Precipitation.* D. Reidel, 714 pp.

Rasmussen, R. M., and H. R. Pruppacher, 1982: A wind tunnel and theoretical study of the melting behavior of atmospheric ice particles. I: A wind tunnel study of frozen drops of radius < 500 μm. *J. Atmos. Sci.*, **39,** 152–158.

——, and A. J. Heymsfield, 1987a: Melting and shedding of graupel and hail: Part II. Sensitivity study. *J. Atmos. Sci.*, **44,** 2764–2782.

——, and ——, 1987b: Melting and shedding of graupel and hail: Part III. Investigation of the role of shed drops as hail embryos in the August 1 CCOPE severe storm. *J. Atmos. Sci.*, **44,** 2783–2803.

——, V. Levizzani and H. R. Pruppacher, 1984a: A wind tunnel and theoretical study of the melting behavior of atmospheric ice particles. II: A theoretical study for frozen drops of radius < 500 μm. *J. Atmos. Sci.*, **41,** 374–380.

——, —— and ——, 1984b: A wind tunnel and theoretical study on the melting behavior of atmospheric ice particles. III: Experiment and theory for spherical ice particles of radius > 500 μm. *J. Atmos. Sci.*, **41,** 381–388.

Roos, D. v. d. S., 1972: A giant hailstone from Kansas in free fall. *J. Appl. Meteor.*, **11,** 1008–1011.

——, and A. E. Carte, 1973: The falling behavior of oblate and spiky hailstones. *J. Rech. Atmos.*, **7,** 39–52.

Selberg, B. P., and J. A. Nicholls, 1968: Drag coefficient of small spherical particles. *AIAA J.*, **6,** 401–408.

Thwaites, S., J. N. Carras and W. C. Macklin, 1977: The aerodynamics of oblate hailstones. *Quart. J. Roy. Meteor. Soc.*, **103,** 803–808.

Willis, J. T., K. A. Browning and D. Atlas, 1964: Radar observations of ice spheres in free fall. *J. Atmos. Sci.*, **21,** 103–108.

Wisner, C., H. D. Orville and C. Myers, 1972: A numerical model of a hail-bearing cloud. *J. Atmos. Sci.*, **29,** 1160–1181.

Young, R. G., and K. A. Browning, 1967: Wind tunnel tests of simulated spherical hailstones with variable roughness. *J. Atmos. Sci.*, **24,** 58–62.